2020

Fabrication of Dielectric Elastomers with Improved Electromechanical Properties Using Silicone Rubber and Walnut Polyphenols Modified Dielectric Particles

Liang Jiang
Qindao University

Yuhao Wang
Qingdao University

Shipeng Wen
Beijing University of Chemical Technology

Yanfen Zhou
Qingdao University

Qingdao University

See next page for additional authors

Recommended Citation

Jiang, L., Wang, Y., Wen, S., Zhou, Y., Ma, J., Chen, S. & Jerrams, S. (2020). Fabrication of dielectric elastomers with improved electromechanical properties using silicone rubber and walnut polyphenols modified dielectric particles. *Materials and Design*, 192. 108674. doi:10.1016/j.matdes.2020.108674

Materials and Design 192 (2020) 108674

Contents lists available at ScienceDirect

Materials and Design

journal homepage: www.elsevier.com/locate/matdes

Fabrication of dielectric elastomers with improved electromechanical properties using silicone rubber and walnut polyphenols modified dielectric particles

Liang Jiang [a], Yuhao Wang [a], Shipeng Wen [c], Yanfen Zhou [a,*], Jianwei Ma [a], Shaojuan Chen [a,b], Stephen Jerrams [d]

[a] College of Textiles and Clothing, Qingdao University, Qingdao 266071, China
[b] Eco-Textile Collaborative Innovation Center, Qingdao University, Qingdao 266071, China
[c] Beijing Engineering Research Center of Advanced Elastomers, Beijing University of Chemical Technology, Beijing 100029, China
[d] Technological University Dublin (TUD), City Campus, Kevin St, Dublin D08 NF82, Ireland

HIGHLIGHTS

- Walnut polyphenols extracted from walnut husks were used to modify barium titanate (BT) particles.
- The dispersibility of BT in silicone rubber (SR) and the compatibility between BT and SR was improved after modification.
- The SR/WNBT composites achieved the highest actuated area strain of 38%.
- The actuated area strain of SR/WNBT composites exhibited excellent stability during 50 cyclic voltage signals.

GRAPHICAL ABSTRACT

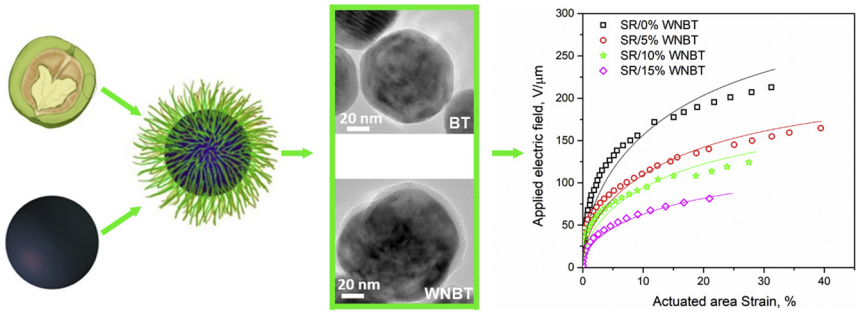

ARTICLE INFO

Article history:
Received 21 January 2020
Received in revised form 21 March 2020
Accepted 23 March 2020
Available online 24 March 2020

Keywords:
Dielectric elastomer
Barium titanate
Coating
Walnut polyphenols
Interface

ABSTRACT

In this work, polyphenolic extract from walnut green husks (denoted as walnut polyphenols), which is an abundant agroindustrial residue/waste, was used to modify barium titanate (BT) particles in the preparation of silicone rubber (SR) based dielectric elastomer (DE) composites with enhanced electromechanical performance. By employing walnut polyphenols modification, the dispersibility of BT particles in the SR matrix and the compatibility between BT and SR were greatly improved, which resulted in enhanced mechanical performance of the DE composites. Dielectric property measurement showed that DE composites containing walnut polyphenols modified BT particles (WNBT) had higher dielectric constants and lower dielectric losses than that of DEs with unmodified BT particles. Furthermore, it was found that the walnut polyphenols modification resulted in decreased dielectric loss tangent of the DE composites, suggesting an improved compatibility between the modified BT particles and SR. Finally, the static and dynamic electromechanical performance of the DE composites were evaluated. The SR/5% WNBT composite achieved the highest actuated area strain of 38% among the SR based composites used in this work. Moreover, the actuated area strain of SR/WNBT composites exhibited excellent electromechanical stability during the application of cyclic voltage signals.

* Corresponding author.
E-mail address: yanfen.zhou@qdu.edu.cn (Y. Zhou).

1. Introduction

High performance actuator materials which can mimic the function of muscle have been sought for biomimetic applications such as micro robots and active prosthetics [1–3]. Dielectric elastomers (DEs) have been considered to offer enhanced properties for soft actuators. These properties include low modulus, high electromechanical coupling efficiency, high actuation strain, high response speed and facile process ability [4,5]. Generally, DEs coated with compliant electrodes can change their shapes when high electric fields are applied. When the electric stimuli are removed, the DEs recover their original shapes [6–12]. The Maxwell stress σ_v, produced by the attraction of negative and positive charges on parallel surfaces, compresses a DE film to transform electrical energy into mechanical energy. σ_v for DEs can be expressed by Eq. (1) [13–15].

$$\sigma_V = \varepsilon'\varepsilon_0(\Phi/h)^2 = \varepsilon'\varepsilon_0\varphi^2 \quad (1)$$

where h is the thickness of the DE, ε' is the dielectric constant of the DE material, ε_0 is the permittivity of free space (8.85×10^{-12} F/m), φ is the electric field which is equal to the applied high voltage (Φ) divided by the thickness of the DE (h).

For small strains (e.g. <20%), the actuated strain is closely related to Maxwell stress and elastic modulus (Y) as expressed by Eq. (2).

$$s_z = -\sigma_V/Y = -\varepsilon'\varepsilon_0\varphi^2/Y \quad (2)$$

For large strains, a number of hyperplastic models, such as Yeoh model, Mooney-Rivlin model, Ogden model and Gent model, et al., are often adopted to study the mechanical performance under electric field [16–18].

The widely used DE materials to date include silicone rubber (SR) [19–21], acrylate [22,23] and thermal plastic polyurethane (TPU) [24,25]. Among these materials, SR is regarded as the most promising candidate for functional DEs [26] because it is capable of attaining large voltage-induced deformations of above 30%, large energy densities and fast response rates. As shown in Eq. (2), the efficient way of reducing the applied electric field of DEs thus saving the energy, is to increase their dielectric constant. It has been found that the incorporation of various high permittivity ceramics [27], such as titanium dioxide (TiO_2) [28–30], lead magnesium niobate-lead titanate (PMN-PT) [31,32] and barium titanate (BT) [33,34], etc., can effectively increase the dielectric constant of DEs. However, the associated problems with doping dielectric fillers are primarily that they generally suffer from high dielectric loss, increase in elastic modulus and poor compatibility with the SR matrix. These issues threaten to limit their wide application [5].

In order to alleviate such problems, a great number of attempts have been made to encapsulate inorganic fillers. These include modification of BT with synthesized chemicals such as phosphonic acid [35], encapsulating conductive polyaniline (PANI) particles into poly(divinyl benzene) (PDVB) [36], coating spherical silver nanoparticles (AgNPs) with thin silica shells [37] and coating BT with γ-methacryloxypropyl trimethoxy silane (KH570) [5]. Kim [35] et al. reported their research on modification of BT using phosphonic acid with obtaining well-dispersed BT nanocomposite films having higher dielectric constant and high dielectric strength. Yang et al. [5] prepared slide-ring materials with high actuated performance incorporating of KH570 modified BT particles. The composite can achieve a large actuated strain of 26% at a low electric field of 12 kV/mm. In their further study, catechol/polyamine co-deposition and subsequent silane γ-(2,3-epoxypropoxy)-propytrimethoxysilane (KH560) grafted BT (BT-PCPA-KH560) was employed to improve the electromechanical properties of natural rubber (NR) dielectric elastomer composites [38]. With the addition of the modified BT particles into NR, a larger actuated strain of 13.4% was achieved, which was about 2.2 times higher than the largest actuated strain of pure NR (6.0%). Among these modification methods, some of the chemicals used are toxic so could harm the environment and humanity, while others are of high cost. Recently, inspired by the bioadhesion principle of marine mussels, it was found that dopamine, which is a kind of catechol derivative, could be spontaneously polymerized under alkaline conditions, leading to the formation a poly(dopamine) (PDA) coating with latent reactivity on a variety of substrates [39]. Due to its simplicity and good biocompatibility, PDA has recently attracted great interest and was intensively studied for surface modification of various materials including the fillers for fabricating DEs [40]. However, PDA has the disadvantages of requiring chemical synthesizing and high cost.

Walnut is a valuable crop, which is cultivated for its fruit and wood. The abundant walnut green husk has been used in a number of industries which exploit the facile extraction process. As the extractions of walnut green husk contain large amounts of phenolic compounds, polyphenol oxidase in walnut catalyzes the oxidation of phenolic compounds into highly reactive quinones which will crosslink with proteins or polymerize generating dark-colored melanins [41]. Traditionally, the application of walnut polyphenols has mainly focused on human health and lifestyle-related diseases such as arteriosclerosis, hypercholesterolemia, cardiovascular disease and cancer [42,43]. Recently, it has been considered as a sustainable and cheap potential candidate for the surface modification of mesoporous carbon nanospheres [44]. However, the use of walnut green husk extracts in modifying the surface of dielectric particles to prepare dielectric elastomer composites has been unreported to date. Therefore, this paper delineates a facial method of modifying the surface of BT particles with the aim of preparing DE composites with enhanced electromechanical properties. The influence of walnut polyphenols modification on the particle dispersion, mechanical properties, dielectric properties and electromechanical properties of silicone based DE composites was investigated. In particular, the dynamic electromechanical properties of the DE composites were evaluated.

2. Experimental

2.1. Materials

Walnut green husks were purchased from Hangzhou Linran Biotechnology Co., Ltd., China. Two-component silicone LSR 4305 was provided by Bluestar Ltd., USA. $BaTiO_3$ microparticles with a density of 6.0 g/cm^3 and an average diameter of 50 nm were supplied by Nantong New Electronic Technology Co., Ltd., Jiangsu Province, China. Ethanol and deionized water were purchased from Maclin China. The commercially available conductive carbon grease NYOGEL 756 G, used as the compliant electrode in this work, was provided by Nye Lubricants, Inc., Fairhaven, MA, USA.

2.2. Extraction of walnut polyphenols from walnut green husks

Firstly, walnut green husk powder (6 g) was immersed in ethanol solution (150 ml) with a concentration of 40% (volume fraction). The mixture was treated with ultrasonication at 60 °C for 30 min and then filtered. Subsequently, the solution obtained was transferred into a centrifugal tube and centrifuged for 20 min at a speed of 6000 rev/min; the supernatant liquid was separated and transferred into another tube and centrifuged. This procedure was repeated three times and the extracts obtained were used for the surface modification of $BaTiO_3$ particles.

2.3. Surface modification of $BaTiO_3$ particles

10 g $BaTiO_3$ particles were added to the phenolic compound solution (80 ml) described in the previous paragraph and magnetically stirred at room temperature for 48 h. Then, the mixture was transferred into a tube and centrifuged for 20 min at 6000 rev/min. The supernatant liquid was removed and the centrifuged substrate was washed three times

with deionized water under ultrasonication for 5 min. Finally, the particles obtained were dried in a vacuum oven for 12 h and then fully ground with an agate grinder. The surface modified $BaTiO_3$ is denoted as WNBT while the pristine $BaTiO_3$ is denoted as BT in the remainder of this text.

2.4. Preparation of dielectric elastomer composites

The two components of SR were mixed at a weight ratio of 1:1 and dissolved in heptane. Then, BT or WNBT particles were added to the solution with different contents by weight of 0%, 5%, 10% and 15%. In order to achieve uniform dispersion of the SR and fillers in heptane, the solutions were subjected to ultrasonic shaking for 20 min. Finally, the mixtures were coated on glass with controlled thicknesses by using blade coating and heated at 80 °C for 6 h. The preparation procedure for WNBT and SR/WNBT composites is illustrated schematically in Fig. 1.

2.5. Characterization

The surface chemical compositions of BT and WNBT microparticles were determined by using Fourier transform infrared (FTIR) spectroscopy (Bruker TENSOR27, Germany) and X-ray photoelectron spectroscopy (XPS). XPS measurements were carried out on a Thermo ESCALAB 250XI system (Thermo Electron Corporation, USA) with an Al Ka X-ray source (1486.6 eV photons). The core-level signals were obtained at a photoelectron take-off angle of 45° with respect to the sample surface.

Study of the thermal behavior of BT and WNBT was conducted on a DSC/TG analyzer (STA 449 F3, Netzsch, Germany). The temperature ranged from 40 °C to 800 °C with a heating rate of 20 °C/min.

Surface morphologies of the BT and WNBT microparticles were observed by using a high-resolution transmission electron microscope (HRTEM) (JEM2100F, JEOL, Japan) operating at a voltage of 200 kV. The morphologies of the SR composites filled with BT and WNBT particles were investigated by using a scanning electron microscope (SEM) (VEGA3, TESCAN, Czech Republic) which was equipped with an EDX (E1856-C2B, EDAX, USA).

Tensile tests on the fabricated DE membranes were performed using Instron 5965 tensile apparatus (Boston, MA, USA). Rectangular specimens having a gauge length of 40 mm and gauge width of 10 mm were used. The crosshead speed was 100 mm·min^{-1}. The elastic moduli were determined from the slope of the stress-strain curve using a linear fit to the data points obtained within 10% strain. Dynamic mechanical analysis was carried out on a Q800 DMA (TA Instruments, USA) in the tensile mode. Strips of 5 mm width, 15 mm long, and approximately 0.3 mm thickness were analyzed in a low frequency range from 1 to 10 Hz at room temperature.

A swelling test was carried out in toluene at room temperature for measuring the total crosslink density (n) of the specimens using the Flory-Rehner equation as given in Eq. (3) [45].

$$n = \frac{-\left[\ \ln(1-v_2) + v_2 + \chi_1 {v_2}^2\right]}{V_1\left[{v_2}^{1/3} - v_2/2\right]} \tag{3}$$

where v_2 is the volume fraction of polymer in the swollen mass, V_1 is the molar volume of the solvent and χ_1 is the Flory-Huggins polymer–solvent dimensionless interaction term.

Dielectric measurements of SR/BT and SR/WNBT films were conducted on a broadband dielectric spectrometer (Novocontrol BDS 40, Germany) at 20 °C in the frequency range of 0.1 Hz to 10 MHz. The

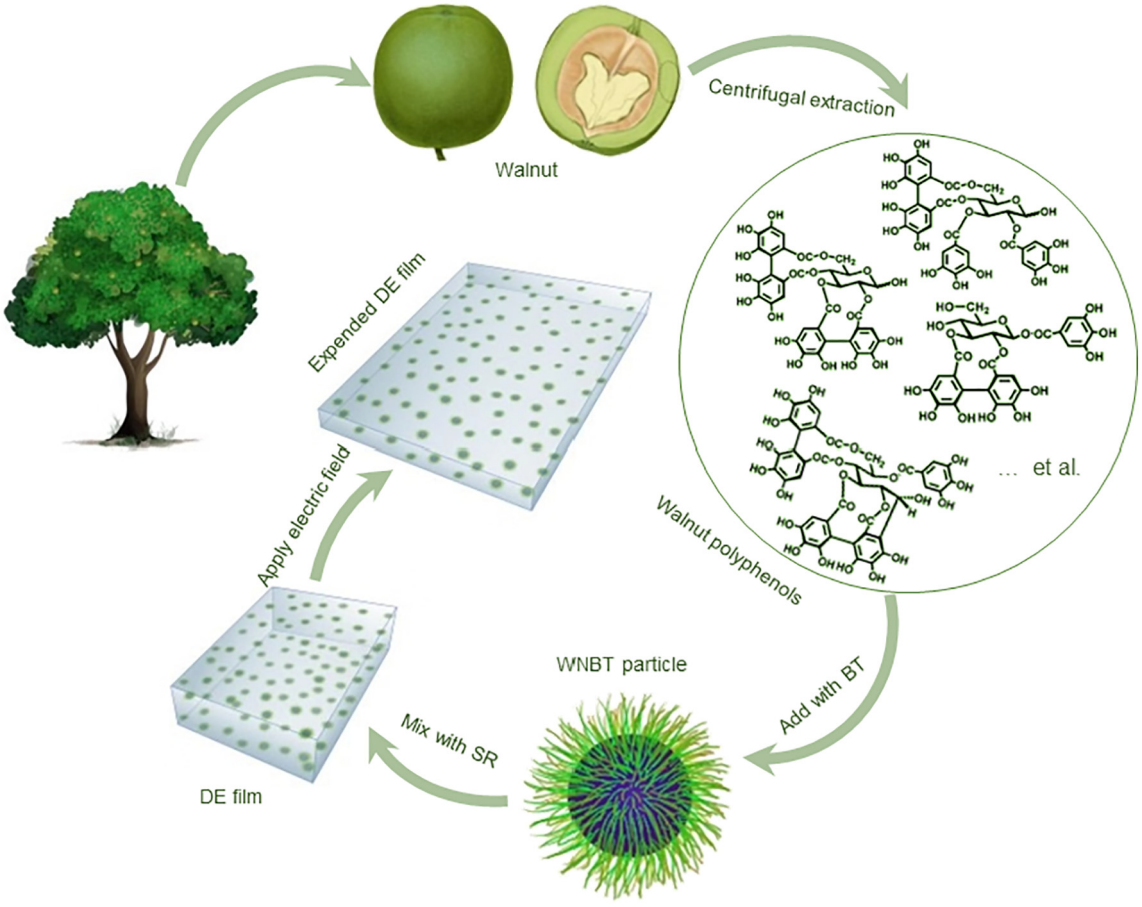

Fig. 1. Schematic illustration of the procedure for preparing WNBT and SR/WNBT composites.

film of approximately 0.3 mm thickness was placed on a cell which comprised a disposable gold-plated flat electrode with a diameter of 20 mm and thickness of 2 mm.

The actuated strain tests were performed by using an electromechanical testing system consisting of a high voltage power supply, a camera and a test rig which was essential to equi-biaxially clamp samples. The testes were performed using circular DE membranes with a diameter of 40 mm and a thickness of approximately 0.3 mm at ambient conditions. The dielectric elastomer films were initially fixed on the circular frames with a prestretch of 2.0. Prior to testing, the samples were coated with the compliant electrode to a diameter of 12 mm on each side. The camera recorded the changes in area when an electric field was incrementally applied in voltage steps of 0.2 kV at 3 s intervals until electric breakdown occurred. Concurrently, the initial area (A_0) and the actuated area (A_1) were measured automatically using LabVIEW. The area strain (s_a) was calculated from Eq. (4).

$$s_a = (A_1 - A_0)/A_0 \tag{4}$$

For mechanical properties, dielectric properties and electromechanical strain tests, each experimental data point was the average of the results obtained from at least three samples under the same conditions.

3. Results and discussion

3.1. Surface modification of BT using walnut polyphenols

The surface chemical composition of BT particles with and without walnut polyphenols modification was analyzed by using XPS. Fig. 2 (a) and (b) shows the wide scan XPS results of BT particles and WNBT particles respectively. The small amount of carbon reading (283.8 eV) in the spectrum of BT particles can be attributed to the small carbonate remaining during the synthesis of barium titanate. Figs. 2(c) and (d) shows the O 1s core level spectrum of BT and WNBT particles respectively. The O 1s core-level spectrum for BT and WNBT particles can be curve-fitted with two peak components: one peak at 531 eV was attributed to the hydroxyl (—O—H) groups and the other one at 533.07 eV attributed to the carbonyl (—C═O) groups. The —O—H and —C═O groups for BT particles was 19.91% and 1.13% respectively, while they increased to 30.9% and 15.0% respectively for WNBT particles. The remarkable increase of the hydroxyl and carbonyl groups indicates that walnut polyphenols have been successfully deposited on the surface of BT particles.

The presence of walnut polyphenols on the BT surface was further confirmed by using FTIR. As can be seen from Fig. 3(a), both the spectrum of BT and WNBT showed peaks at 3431 cm^{-1} and 1621 cm^{-1}, which was assigned to the O—H stretching vibrations and O—H bend vibrations respectively. These peaks might be generated from the ethanol-water contained in the samples [46]. A strong absorption peak appearing at 562 cm^{-1} was ascribed to the vibration of the Ti—O bond. The peak at 1427 cm^{-1} clearly indicates the existence of acetate groups bonded to barium atoms [47] and also suggests symmetric stretching vibrations of carboxylate groups [48]. Compared to BT particles, the spectrum of WNBT particles show new peaks at 1046 cm^{-1}, 2845 cm^{-1} and 2920 cm^{-1}. The peak around 1046 cm^{-1} indicated the C—O stretching vibrations [49] which were generated from ether groups of walnut polyphenols. The peaks at 2924 cm^{-1} and 2850 cm^{-1} corresponded to the dominant antisymmetric and symmetric stretching vibrations of the lipid acyl CH_2 groups [50]. These outcomes further proved that walnut polyphenols successfully deposited on the surfaces of BT particles.

TG analysis was employed to quantify the amount of the polyphenols on the surface of BT particles. Fig. 3(b) presents the thermogravimetric curves of BT and WNBT particles. It can be seen that the total weight loss for a temperature range from 40 °C to 800 °C in the TG curves for BT and WNBT particles was 3.5% and 5.2%, respectively. The weight loss of 0.6% at 100 °C for both BT and WNBT particles was due to the elimination of water absorbed on the surface. The weight loss for BT particles in the temperature range from 100 °C to 800 °C was mainly ascribed to the dehydration from the –OH bonds incorporated in the lattice and elimination of CO_2 from the contaminated $BaCO_3$. However, the weight loss of WNBT particles was 1.7% higher than that of BT particles due to the thermal decomposition of the polyphenols layer on WNBT particles.

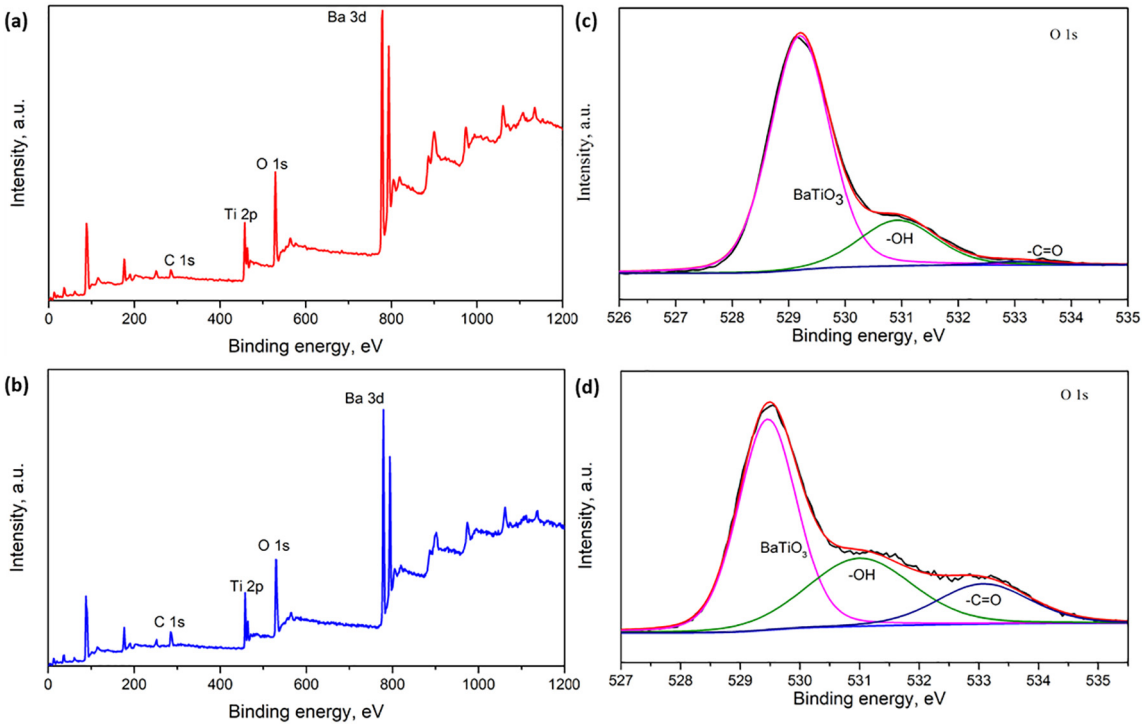

Fig. 2. XPS Wide scan of (a) BT particles and (b) WNBT particles; O 1s core level of (c) BT particles and (d) WNBT particles

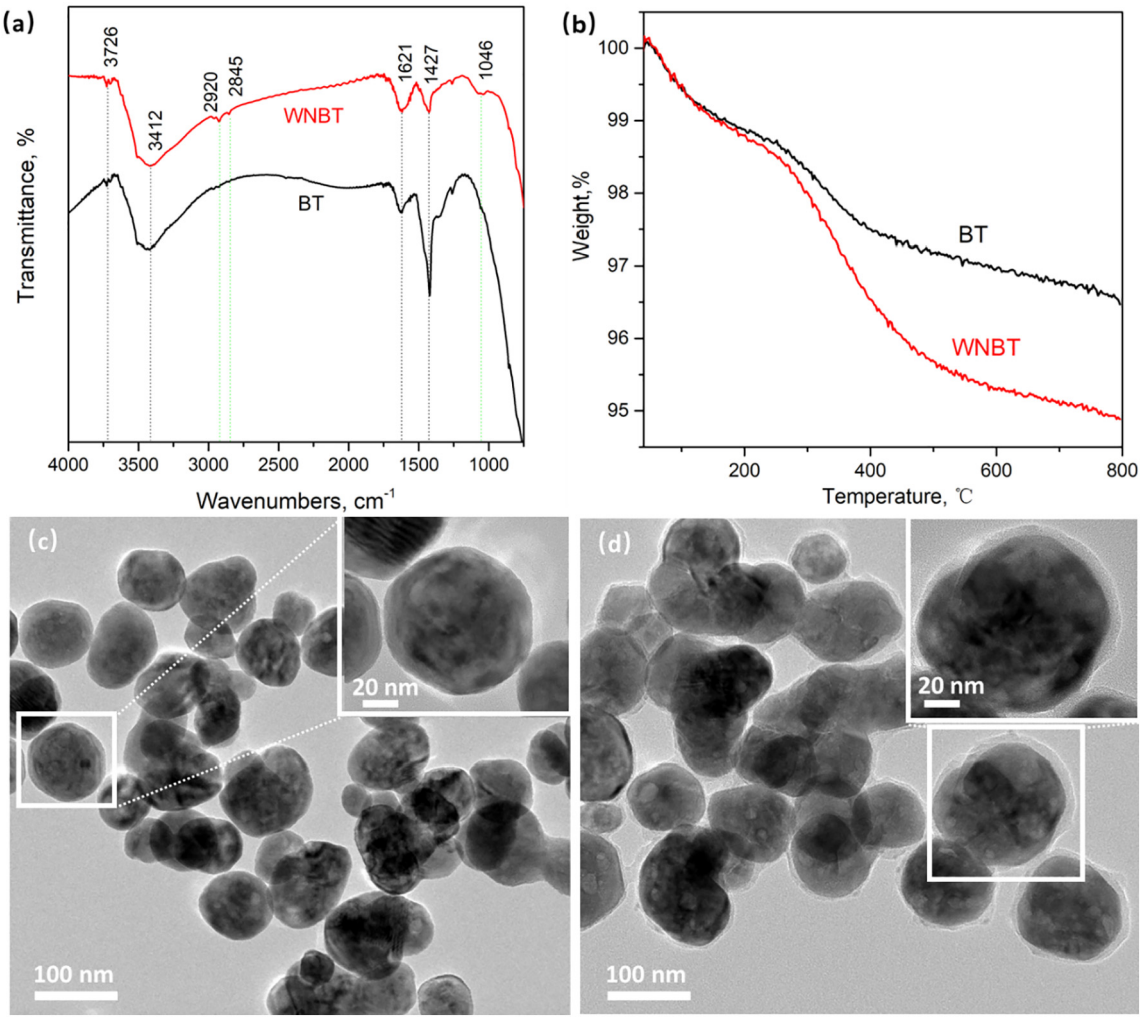

Fig. 3. (a) The FTIR spectrum of BT and WNBT and (b) the TG curves for BT and WNBT; The TEM images of (c) BT and (d) WNBT.

TEM was used to observe the coating morphology of the walnut polyphenols on the BT particle surface. From Fig. 3(c) and (d), it can be seen that BT and WNBT particles were dispersed evenly with diameters ranging from 20 to 50 nm. The distinct layer of walnut polyphenols coating can be observed clearly from Fig. 3(d); the thickness of the coating layer was about 7.2 nm.

Fig. 4 (a_0-f_0) presents the cross-sectional morphology of DE composites with different BT and WNBT contents. It can be seen that for DE composites with pristine BT, many large agglomerations of BT nanoparticles were exposed on the fractured surfaces. The amount of agglomerations increased with increasing the BT content. This is due to the poor dispersibility of the nanoparticles in the silicone rubber matrix. The EDX mapping of Ti element shown in Fig. 4 (a_1-f_1) also clearly showed agglomerations existed in SR based composites and the poor dispersion of the BT particles, indicating that the interfacial interaction between the BT particles and SR was weak. In contrast, the DE composites filled with WNBT exhibited significantly improved filler dispersibility, even at a WNBT content of as high as 15%. This may be explained by the fact that the large amount of hydroxyl groups in walnut polyphenols coated on BT particles provided more active sites to form hydrogen bonds, leading to an enhanced interfacial interaction between WNBT and SR, thus significantly improving the dispersibility of WNBT particles in SR matrix [51]. Additionally, it can be easily observed that the interface between the WNBT particles and matrix was blurred, revealing a good compatibility between WNBT particles and the silicone matrix.

3.2. Mechanical properties of DE composites

The mechanical properties of SR composites filled with different amounts of BT and WNBT particles were investigated and the results are presented in Fig. 5. It can be seen from the figure that the tensile strength and elongation at break of pure silicone rubber were about 1.27 ± 0.14 MPa and 1073 ± 62% respectively. It is not surprising to see that tensile strength of the SR based composites increased with increasing filler content for either BT or WNBT particles, confirming that the incorporation of both BT and WNBT particles reinforced the silicone rubber. However, for the same amount of filler content, the tensile strength of the SR/WNBT composites was higher than that of the SR/BT composites due to the enhanced interfacial interaction between them. The molecular chains for the SR/BT composites moved easily due to the weak interfacial interaction, while the movement of the chains for the SR/WNBT composites was restricted due to the strong interfacial interaction which further led to the uniform distribution of external force [52]. In addition, it was found that the elongation at break for the SR/BT and SR/WNBT composites was higher than that of the pure SR. This was ascribed to the decrease in crosslink density with the addition of fillers as shown in Fig. 5. With the increase of filler content, the elongation at break changed for both the SR/BT composites and the SR/WNBT composites. It might be determined by the competition between crosslink density effect and reinforcing effect: on the one hand, the inorganic BT or WNBT particles acted as physical crosslinks

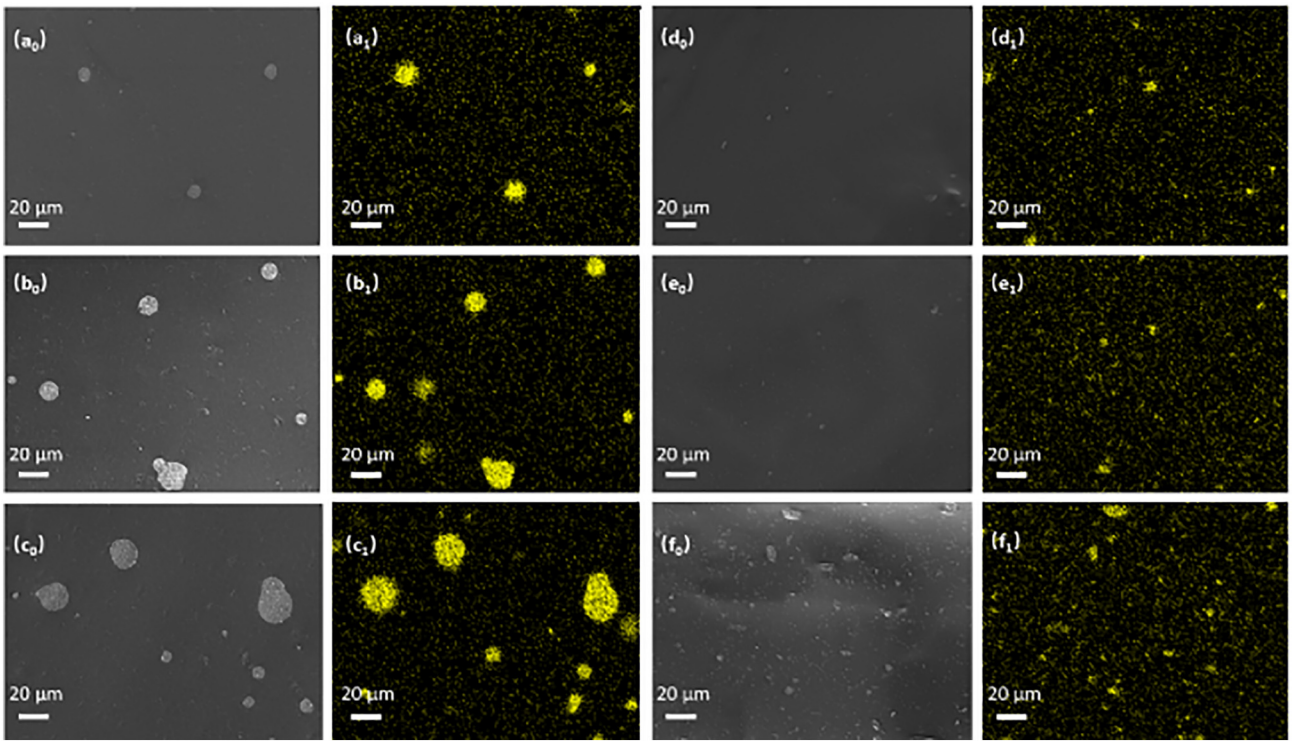

Fig. 4. SEM images of (a_0) SR/5%BT, (b_0) SR/10%BT, (c_0) SR/15% BT, (d_0) SR/5% WNBT, (e_0) SR/10% WNBT, (f_0) SR/15% WNBT and SEM-EDX chemical mapping of Ti in (a_1) SR/5% BT, (b_1) SR/10% BT, (c_1) SR/15% BT, (d_1) SR/5% WNBT, (e_1) SR/10% WNBT, (f_1) SR/15% WNBT.

in the SR matrix to cause a reinforcing effect and hindered the mobility of polymer chains [53], which contributed to the reduction in elongation and on the other hand, the decreased crosslink density with the increase in filler content led to the increase in elongation at break. The SR/10% BT composites showed the highest elongation at break among all the SR/BT composites. This is mainly because the decreased crosslink density played a dominant role in the increase of elongation at break when the BT content was below 10%. However, with the addition of BT particles above 10%, more physical crosslinks were formed, which restricted the mobility of polymer side chains and consequently resulted in decreased elongation at break. For the SR/WNBT composites, though the crosslink density also decreased with the increasing filler content, the walnut polyphenols modification rendered more organic molecules

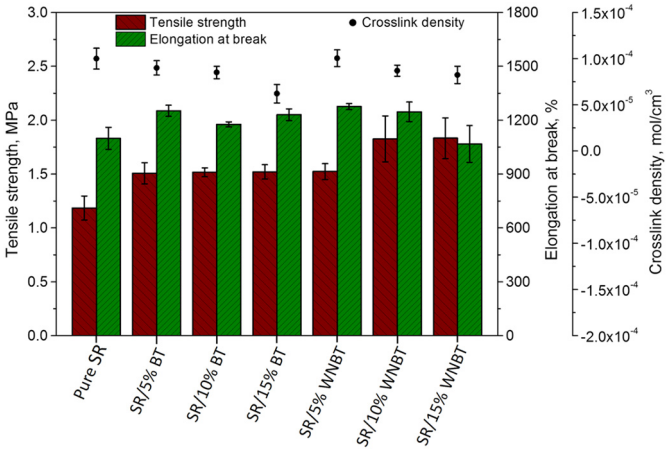

Fig. 5. The tensile strength, the elongation at break and the crosslink density of DEs with various contents of BT and WNBT particles.

to bond to the BT particle surface and thus further restricted the deformation of the composite. The elongation at break of SR/WNBT was therefore lower than that of SR/BT with the same amount of particle content.

Pre-stretch plays a significant role in the electromechanical properties of DEs such as decreasing the applied voltage by thinning DEs and increasing the breakdown field. Previously, we have found that the elastic modulus, which is a key factor for electromechanical properties of DEs as stated before, can be tuned by breaking the entanglement of molecular chains using pre-stretch. Thus, the relation between the secant modulus, an alternative indication of elastic moduli, and the stretch was investigated here. The curves of secant modulus versus strain for SR/BT and SR/WNBT composites are depicted in Fig. 6(a) and (b), respectively. It can be seen that the secant modulus of DE composites increased with the increasing BT and WNBT content. It could be explained that with the addition of more BT particles, more physical crosslinks were formed which restrained the mobility of side chains of the SR molecules. The secant modulus for SR/WNBT composites was higher than that of SR/BT composites with the same filler content. This is probably due to more SR molecules surrounding the BT particles when they were coated with a layer of walnut polyphenols. Furthermore, it can be seen that the secant modulus-strain curves exhibited a material specific minimum in modulus, indicating that their stiffness can be reduced by pre-stretching to small ratios. This phenomenon is considered to be a result of the intermolecular forces and chain entanglements between particles and matrices [4]. The minimum elastic moduli were observed at strains of around 100% for both SR/BT and SR/WNBT composites. This means that the application of an external force initially unraveled chain entanglements and resulted in the decrease in elastic modulus at small strains. Thereafter, as the stretch ratio increased, intermolecular forces increased due to the hydrogen bonds formed between WNBT particles and SR accompanied by the reorientation of molecular chains. In line with Eq. (2), it is likely that a maximum voltage-induced area strain from pre-stretching can be obtained at a stretch ratio close to 2.0.

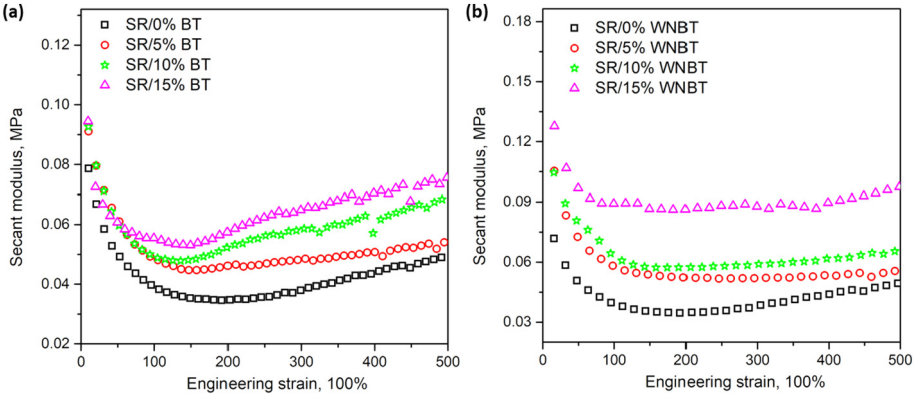

Fig. 6. The change of secant modulus with increasing strain for DE composites with (a) BT and (b) WNBT.

3.3. Dielectric properties

When subjected to high external electric fields, the dipoles in DEs are reoriented, thus inducing them to deform. This phenomenon is often called "polarizability". The polarizability of DEs can be studied by using dielectric spectra. Fig. 7 shows the spectra of dielectric constant and dielectric loss tangent related to frequency for SR/BT and SR/WNBT composites. As can be seen, the pure SR had the lowest dielectric constant of 2.9 at a frequency of 1 kHz. The addition of the dielectric BT or WNBT particles resulted in the increase in the dielectric constant. For the same content of fillers, the dielectric constants of the DE composites filled with WNBT particles were higher than those of the composites containing BT particles. This is mainly because the interfacial polarization was enhanced by the improved interface compatibility between

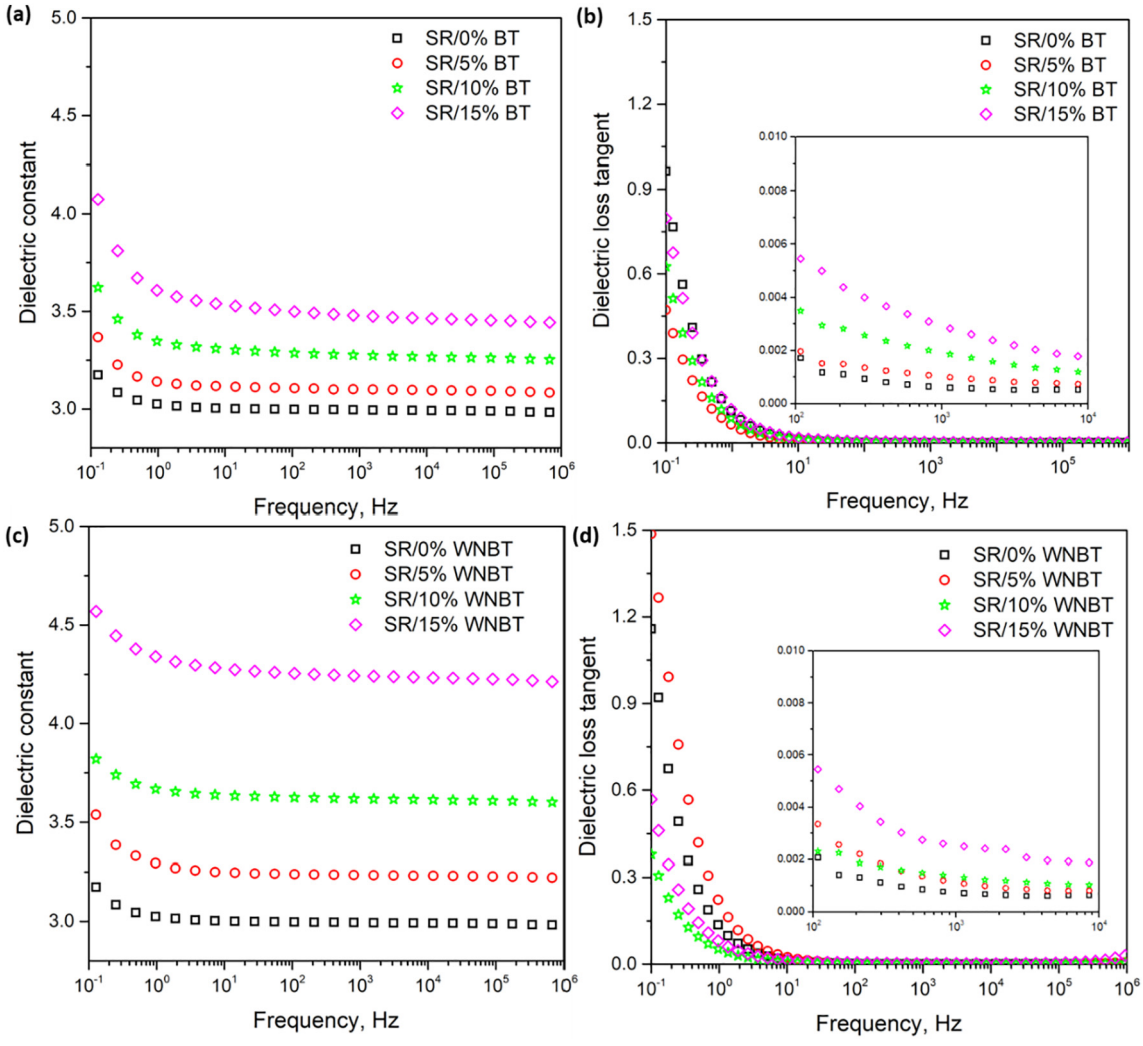

Fig. 7. Dielectric constant as a function of frequency for (a) SR/BT composites and (c) SR/WNBT composites; dielectric loss tangent as a function of frequency for (b) SR/BT composites and (d) SR/WNBT composites.

SR and BT after walnut polyphenols modification [54]. The change of dielectric loss shown in Fig. 7(b) and (d) demonstrates that the dielectric loss decreased with increasing frequency for both SR/BT and SR/WNBT composites. In distinct contrast, for the same particle loading, the dielectric loss tangent at a frequency of 1 kHz was lower for SR/WNBT composites than that of SR/BT composites. Similar results have been reported that the formation of strong interfacial bonding between fillers and matrices after surface modification decreased the dielectric losses of DEs [55]. This can be explained by the fact that the surface modification of dielectric BT particles reduced the occurrence of particle agglomeration and concurrently prevented electrons from conducting which consequently resulting in a low leakage current [56].

Table 1
The maximum actuated area strain and electromechanical sensitivity of the materials used in this research.

Sample	Maximum actuated area strain (%)	Electromechanical sensitivity (MPa^{-1})
Pure SR	32	35
SR/5% BT	24	34
SR/10% BT	19	36
SR/15% BT	18	37
SR/5% WNBT	38	28
SR/10% WNBT	28	31
SR/15% WNBT	25	32

3.4. Actuated strain of dielectric composites

DEs are smart materials that are sensitive to electric field. As shown in Fig. 8(a), when a high electric voltage was applied on a pre-stretched DE film coated with compliant electrodes on the top and bottom surfaces, the DE expanded in area and compressed in thickness. The actuated strain of DEs showed a dependence on the applied electric field. As can be seen from Fig. 8(b) and (c), it can be seen that the actuated area strain of SR and SR based DE composites with BT and WNBT particles was increased by increasing the applied electric field. The pure SR produced a rather high voltage induced deformation of up to 32% for an electric field of 210 V/μm. The incorporation of BT reduced the field-induced area strain at break. Moreover, the field-induced strain at break decreased with the increasing filler content for SR/BT composite, as shown in Table 1. However, the maximum actuated area strain for SR/WNBT composites was 38% at the electric field of 187 V/μm with the addition of 5 wt% WNBT which is higher than that for the pure SR. It is worth noting that, by comparison with SR/BT composites, the maximum actuated strain for SR/WNBT composites was larger for the same filler content, and the electric filed strength that was required for achieving the same actuated stain was lower for SR/WNBT composites. For example, to achieve a 15% field-induced area strain, the electric field strength for pure SR was about 177 V/μm, but it was only 138 V/μm for SR/5% BT and even lower at 125 V/μm for SR/5% WNBT. The likely cause for these changes is that the enhancement of dielectric constant with the addition of the dielectric BT particles and the further increase in dielectric constant after BT particles were functionalized with walnut polyphenols abated the applied electric field.

Numerical analysis of transferring the electrical energy of DEs to mechanical work is an important feature of the investigation of DEs' electromechanical performance. In order to do this, it was necessary to introduce a suitable mechanical model to provide a credible extrapolation of the stress-strain curve and hence an improved understanding of stress-stretch behavior at larger equi-biaxial stretch ratios. The Gent hyperelastic material model belongs to the category of

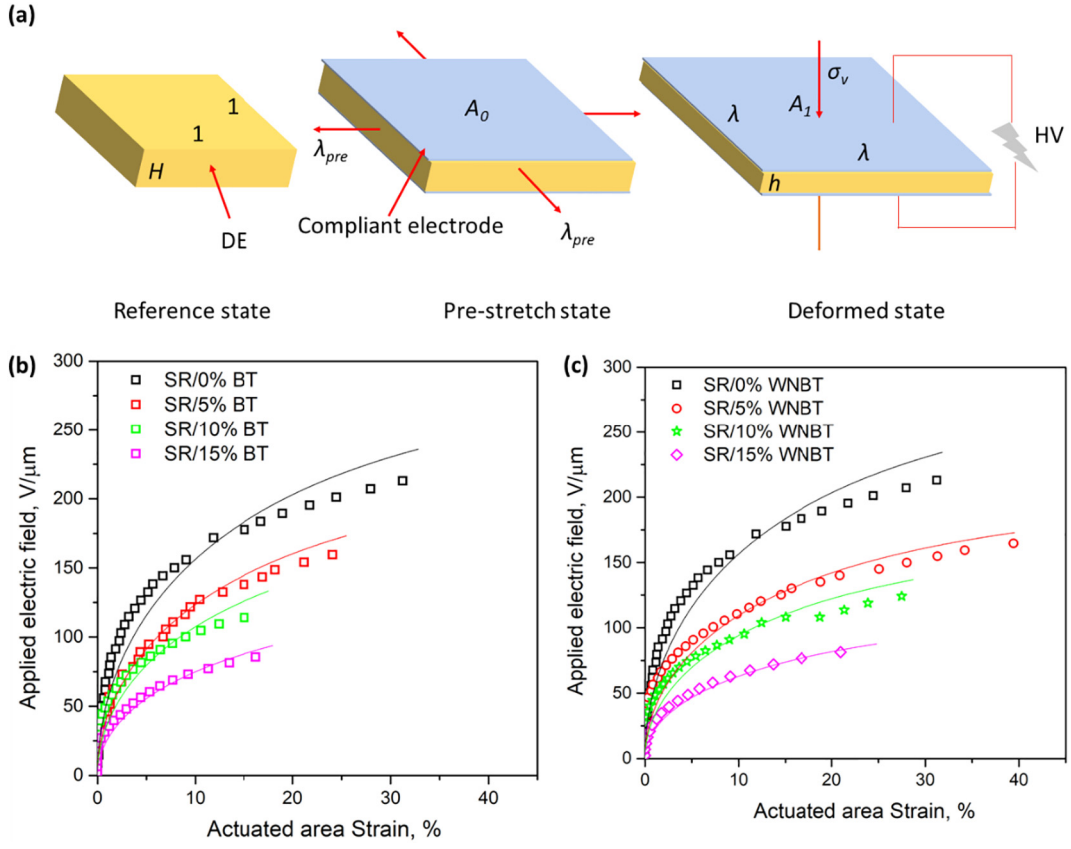

Fig. 8. (a) The working principle of DEs (b) the plots of actuated area strain related to applied electric field for SR/BT composites; (c) the plots of actuated area strain related to applied electric field for SR/WNBT composites.

phenomenological models of rubber elasticity and is based on the concept of limited chain extensibility. The strain energy function is given as [57,58]:

$$W = -\frac{\mu J_m}{2} \ln\left(1-\frac{I_1-3}{J_m}\right) \tag{5}$$

where μ is the shear modulus, J_m is a dimensionless material constant associated with the limiting stretch and I_1 the first even-powered strain invariant which is given by:

$$I_1 = 2\lambda^2 + \frac{1}{\lambda^4} \tag{6}$$

where λ is the stretch ratio.

This model (Eq. (5)) represents the stiffening of the material at large strains within acceptable accuracy. It has the advantage of mathematical simplicity and allows detailed analysis and explicit solutions of particular boundary-value problems.

Meanwhile, the true stress-strain relationship $\sigma(\lambda)$ for elastomers can be derived from a strain energy density function [59] as shown in Eq. (7).

$$\sigma(\lambda) = \lambda\frac{\partial W(\lambda)}{\partial \lambda} \tag{7}$$

where W is work done per unit volume and σ is engineering stress.

According to Suo's theory [60], the applied voltage Φ is a function of stretch λ which can be obtained from Eq. (8) [61].

$$\sigma_{pre} + \sigma_V = \sigma(\lambda) \tag{8}$$

If the membrane is subjected to a fixed force P and is mechanically pre-stretched to a ratio λ_{pre} with the side and thickness changing to L_1 and H respectively corresponding to a stress $\sigma_{pre} = P/L_1H$ by substituting Eqs. (5), (6) and (7) into Eq. (8), an expression for true stress can be obtained:

$$\frac{P}{L_1H} + \varepsilon'\varepsilon_0\lambda^3\left(\frac{\Phi}{H}\right)^2 = \frac{\mu\left(\lambda-\lambda^{-5}\right)}{1-\left(2\lambda^{-5}+\lambda^{-5}-3\right)/J_m} \tag{9}$$

Finally, the applied electric field φ which is equal to the applied high voltage (Φ) divided by the original thickness of the DE (H) can be determined using the expression:

$$\varphi = \frac{\Phi}{H} = \sqrt{\left(\frac{\mu\left(\lambda-\lambda^{-5}\right)}{1-\left(2\lambda^{-5}+\lambda^{-5}-3\right)/J_m} - \frac{P}{L_1H}\right)/\varepsilon'\varepsilon_0\lambda^3} \tag{10}$$

For a commercial DE material VHB 4910, its elongation at break is approximately 1000% when $J_m = 125$. This value was taken for the SR based DE materials in the present study. It can be seen from Fig. 8 (b) and (c) that the Gent model correlates well with the experimental data.

As mentioned previously, Eq. (2) suggests that electric field actuated performance of DE composites is determined by elastic modulus and dielectric constant. The parameter of dielectric constant divided by elastic modulus is termed the electromechanical sensitivity [5]. Generally, DE films with high electromechanical sensitivity have the ability to achieve large voltage-induced deformations. The electromechanical sensitivity for both the SR/BT composites and the SR/WNBT composites is shown in Table 1. It was observed that SR/15% BT showed the highest electromechanical sensitivity of 37 MPa^{-1}, compared to that of 32 MPa^{-1} for SR/15% WNBT composite and 35 MPa^{-1} for pure SR. For the SR/BT composites or the SR/WNBT composites, the lowest electromechanical sensitivity was obtained with a filler content of 5%. It can also be seen that the electromechanical sensitivity of SR/BT composites was slightly higher than that of SR/WNBT composites. According to Eq. (2), the SR/BT composites should possess larger voltage induced area strain. However, the large amount of agglomerates in SR/BT composites greatly lowered the electrical breakdown field and thus inhibited the samples from producing larger actuated area stain [62]. As a consequence, the SR/BT composites showed lower actuated area strain than the SR/WNBT composites.

Those results above showed that all the fabricated SR/BT and SR/WNBT composites had actuated area strain of above 15% with applied electric fields below 200 V/μm, indicating the improved static electromechanical performance of these materials. In order to evaluate their dynamic electromechanical performance, cyclic driving voltages were applied to actuate DE composites to produce tensile area strain amplitudes from a zero minimum to approximately 10%. Fig. 9(a), (b) and (c) shows the variations of actuated area strain during 50 repeated cycles for the pure SR, SR/10% BT and SR/10% WNBT composite, respectively. In order to obtain a voltage induced strain of 10%, a maximum applied electric field of 150 V/μm was applied for the pure SR, 105 V/μm for SR/10% BT and 90 V/μm for SR/10% WNBT. For the pure SR, as shown in Fig. 9(a), the maximum actuated strain at the 50th cycle was about 1% larger than that in the first cycle suggesting a good stability. From Fig. 9(c) it can be seen that the SR/10% WNBT composite had a more stable deformation under an applied driving voltage for all cycles. However, for SR/10% BT shown in Fig. 9(b), it is observed that the latter cycles had higher peaks than the initial cycles. The maximum actuated strain at the 50th circle was 2% larger than that in the first cycle. This is due to the enhanced energy loss caused by the hysteresis during compression in thickness under the electrostatic force for SR/10% BT composite. The viscoelasticity of DE composites containing BT and WNBT particles was determined by DMA analysis. Fig. 9(d) and Fig. 9 (e) show the plots of storage modulus and tangent delta related with frequency for the pure SR, SR/10% BT and SR/10% WNBT composites. It can be seen that the storage modulus increased with the increasing frequency from 0.01 Hz to 10 Hz for all the materials. Whereas in contrast, the storage modulus of SR/10% WNBT was higher due to improved dispersibility of WNBT particles in SR and the enhanced compatibility between them. Furthermore, tangent delta of SR/10% BT was the largest among them, proclaiming the largest hysteresis loss because of the poor interfacial interactions between BT particles and the SR matrix.

4. Conclusions

SR based DE composites having improved eletromechanical performance were developed by employing walnut polyphenols modified $BaTiO_3$ nanoparticles as dielectric fillers. It was found that the walnut polyphenols coating on the surface of $BaTiO_3$ particles had a thickness of approximately 7.2 nm and a weight ratio of around 1.7%. The walnut polyphenols modification remarkably improved the dispersibility of BT particles in the SR matrix. The resultant DE composites with walnut polyphenols modified BT particles showed enhanced tensile strength compared with DEs with pristine BT particles. The dielectric property test demonstrated that the resultant DEs also had higher dielectric constants and lower dielectric losses than those of DEs with unmodified BT particles because of the enhanced interfacial polarization. These properties are beneficial for designing higher voltage-induced deformation of DE composites. The SR/WNBT composite showed higher actuated area strain than the SR/BT composites. Dynamic electromechanical performance evaluation demonstrated that the SR/WNBT composites had a more stable voltage induced deformation of about 10% more than that of pure SR and SR/BT composites during applying 50 cyclic voltage signals. Combining good mechanical properties, large field-induced deformation and stable dynamic electromechanical performance, the SR/WNBT is a promising candidate for fabricating mimicry and other DE devices.

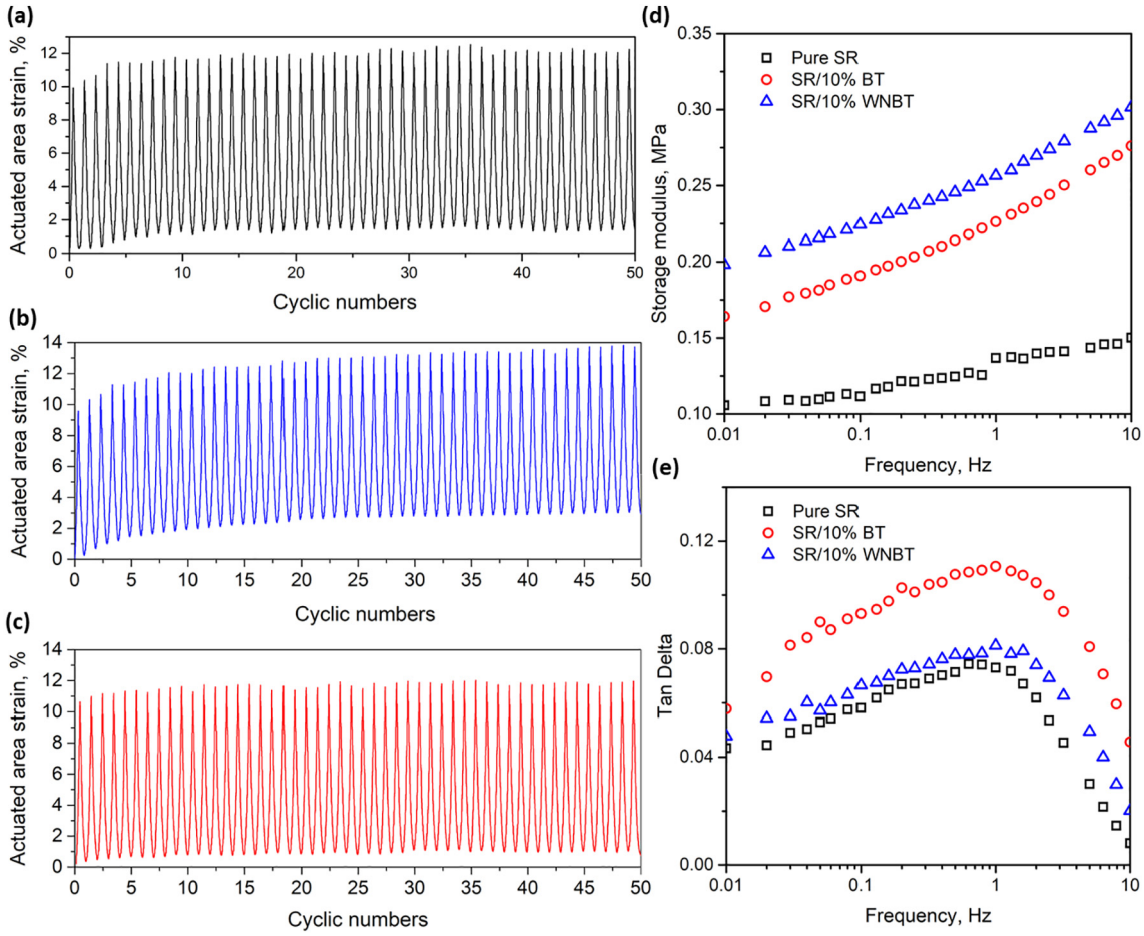

Fig. 9. The electromechanical properties for (a) pure SR subjected to a cyclic electric field of 0–150 V/μm, (b) SR/10% BT composite subjected to a cyclic electric field of 0–105 V/μm and (c) SR/10% WNBT composite under a cyclic electric field of 0–90 V/μm; (d) dynamic storage modulus related to frequency and (e) tangent delta related to frequency for pure SR, SR/10% BT and SR/10% WNBT composites.

CRediT authorship contribution statement

Liang Jiang: Writing - original draft, Writing - review & editing, Conceptualization, Formal analysis, Funding acquisition. **Yuhao Wang:** Writing - original draft, Formal analysis. **Shipeng Wen:** Writing - original draft, Formal analysis. **Yanfen Zhou:** Writing - original draft, Writing - review & editing, Conceptualization, Funding acquisition. **Jianwei Ma:** Project administration, Resources. **Shaojuan Chen:** Writing - original draft, Writing - review & editing, Formal analysis. **Stephen Jerrams:** Writing - review & editing, Conceptualization, Supervision.

Declaration of competing interest

The authors declare that they have no known competing financial interests or personal relationships that could have appeared to influence the work reported in this paper.

Acknowledgements

The authors gratefully acknowledge the National Natural Science Foundation of China (Grant no. 51703108), the National Key Research and Development Program of China (Grant no. 2017YFB0309805-2), the Shandong Provincial Natural Science Foundation, China (Grant no. ZR2017BEM042) and the Shandong Province Key Research and Development Program, China (Grant no. 2019GGX102071 and 2018GGX108003) for financial support.

Data availability

The raw data required to reproduce these findings cannot be shared at this time as the data also forms part of an ongoing study.

References

[1] M. Duduta, E. Hajiesmaili, H. Zhao, R.J. Wood, D.R. Clarke, Realizing the potential of dielectric elastomer artificial muscles, Proc. Natl. Acad. Sci. 116 (2019) 2476–2481.
[2] H. Imamura, K. Kadooka, M. Taya, A variable stiffness dielectric elastomer actuator based on electrostatic chucking, Soft Matter 13 (2017) 3440–3448.
[3] C. Ellingford, C. Bowen, T. McNally, C. Wan, Intrinsically tuning the electromechanical properties of elastomeric dielectrics: a chemistry perspective, Macromol. Rapid Commun. 39 (2018), 1800340.
[4] L. Jiang, A. Betts, D. Kennedy, S. Jerrams, Improving the electromechanical performance of dielectric elastomers using silicone rubber and dopamine coated barium titanate, Mater. Des. 85 (2015) 733–742.
[5] D. Yang, F. Ge, M. Tian, N. Ning, L. Zhang, C. Zhao, et al., Dielectric elastomer actuator with excellent electromechanical performance using slide-ring materials/barium titanate composites, Journal of Materials and Chemistry A 3 (2015) 9468–9479.
[6] R. Pelrine, R. Kornbluh, Q. Pei, J. Joseph, High-speed electrically actuated elastomers with strain greater than 100%, Science 287 (2000) 836–839.
[7] G. Kovacs, L. Düring, S. Michel, G. Terrasi, Stacked dielectric elastomer actuator for tensile force transmission, Sensors Actuators A Phys. 155 (2009) 299–307.
[8] W.-P. Yang, L.-W. Chen, The tunable acoustic band gaps of two-dimensional phononic crystals with a dielectric elastomer cylindrical actuator, Smart Mater. Struct. 17 (2008), 015011.
[9] S. Rosset, M. Niklaus, P. Dubois, H.R. Shea, Performance characterization of miniaturized dielectric elastomer actuators fabricated using metal ion implantation, Micro Electro Mechanical Systems (2008) 503–506IEEE 21st International Conference on Micro Electro Mechanical Systems.

[10] P. Dubois, S. Rosset, S. Koster, J. Stauffer, S. Mikhaïlov, M. Dadras, et al., Microactuators based on ion implanted dielectric electroactive polymer (EAP) membranes, Sensors Actuators A Phys. 130 (2006) 147–154.
[11] S.P. Lacour, H. Prahlad, R. Pelrine, S. Wagner, Mechatronic system of dielectric elastomer actuators addressed by thin film photoconductors on plastic, Sensors Actuators A Phys. 111 (2004) 288–292.
[12] X. Zhao, W. Hong, Z. Suo, Electromechanical hysteresis and coexistent states in dielectric elastomers, Phys. Rev. B 76 (2007), 134113.
[13] A.P. Gerratt, B. Balakrisnan, I. Penskiy, S. Bergbreiter, Dielectric elastomer actuators fabricated using a micro-molding process, Smart Mater. Struct. 23 (2014), 055004.
[14] J. Biggs, K. Danielmeier, J. Hitzbleck, J. Krause, T. Kridl, S. Nowak, et al., Electroactive polymers: developments of and perspectives for dielectric elastomers, Angew. Chem. Int. Ed. 52 (2013) 9409–9421.
[15] Y. Zhang, C. Ellingford, R. Zhang, J. Roscow, M. Hopkins, P. Keogh, et al., Electrical and mechanical self-healing in high-performance dielectric elastomer actuator materials, Adv. Funct. Mater. 29 (2019), 1808431.
[16] C. Tang, W. Ma, B. Li, M. Jin, H. Chen, Cephalopod-inspired swimming robot using dielectric elastomer synthetic jet actuator, Adv. Eng. Mater., doi:https://doi.org/10.1002/adem.201901130.
[17] D. Ahmad, K. Patra, Experimental and theoretical analysis of laterally pre-stretched pure shear deformation of dielectric elastomer, Polym. Test. 75 (2019) 291–297.
[18] T.-J. Kim, Y. Liu, J. Leng, Cauchy stresses and vibration frequencies for the instability parameters of dielectric elastomer actuators, J. Appl. Polym. Sci. 135 (2018), 46215.
[19] P. Brochu, H. Stoyanov, X. Niu, Q. Pei, All-silicone prestrain-locked interpenetrating polymer network elastomers: free-standing silicone artificial muscles with improved performance and robustness, Smart Mater. Struct. 22 (2013), 055022.
[20] F. Carpi, G. Gallone, F. Galantini, D. De Rossi, Silicone–poly(hexylthiophene) blends as elastomers with enhanced electromechanical transduction properties, Adv. Funct. Mater. 18 (2008) 235–241.
[21] H. Liu, L. Zhang, D. Yang, Y. Yu, L. Yao, M. Tian, Mechanical, dielectric, and actuated strain of silicone elastomer filled with various types of TiO2, Soft Mater 11 (2012) 363–370.
[22] M. Wissler, E. Mazza, Mechanical behavior of an acrylic elastomer used in dielectric elastomer actuators, Sensors Actuators A Phys. 134 (2007) 494–504.
[23] N.C. Goulbourne, A constitutive model of polyacrylate interpenetrating polymer networks for dielectric elastomers, Int. J. Solids Struct. 48 (2011) 1085–1091.
[24] M. Tian, Y. Yao, S. Liu, D. Yang, T. Nishi, L. Zhang, et al., Separated-structured all-organic dielectric elastomer with large actuation strain under ultralow-voltage and high mechanical strength, J. Mater. Chem. A 3 (2014) 1483–1491.
[25] C.-P. Chwang, C.-D. Liu, S.-W. Huang, D.-Y. Chao, S.-N. Lee, Synthesis and characterization of high dielectric constant polyaniline/polyurethane blends, Synth. Met. 142 (2004) 275–281.
[26] D.M. Opris, Polar elastomers as novel materials for electromechanical actuator applications, Adv. Mater. 30 (2018), 1703678.
[27] F.B. Madsen, A.E. Daugaard, S. Hvilsted, A.L. Skov, The current state of silicone-based dielectric elastomer transducers, Macromol. Rapid Commun. 37 (2016) 378–413.
[28] H.L. Liu, L.Q. Zhang, D. Yang, Y.C. Yu, L. Yao, M. Tian, Mechanical, dielectric, and actuated strain of silicone elastomer filled with various types of TiO2, Soft Materials 11 (2013) 363–370.
[29] G. Ouyang, K. Wang, X.Y. Chen, TiO 2 nanoparticles modified polydimethylsiloxane with fast response time and increased dielectric constant, J. Micromech. Microeng. 22 (2012), 074002.
[30] F. Carpi, D.D. Rossi, Improvement of electromechanical actuating performances of a silicone dielectric elastomer by dispersion of titanium dioxide powder, IEEE Trans. Dielectr. Electr. Insul. 12 (2005) 835–843.
[31] G. Gallone, F. Carpi, D. De Rossi, G. Levita, A. Marchetti, Dielectric constant enhancement in a silicone elastomer filled with lead magnesium niobate–lead titanate, Mater. Sci. Eng. C 27 (2007) 110–116.
[32] D. Yang, L. Zhang, H. Liu, Y. Dong, Y. Yu, M. Tian, Lead magnesium niobate-filled silicone dielectric elastomer with large actuated strain, J. Appl. Polym. Sci. 125 (2012) 2196–2201.
[33] Z. Zhang, L. Liu, J. Fan, K. Yu, Y. Liu, L. Shi, et al., New silicone dielectric elastomers with a high dielectric constant, Proc. SPIE 6926, Modeling, Signal Processing, and Control for Smart Structures 2008, pp. 692610–692618.
[34] L. Jiang, A. Betts, D. Kennedy, S. Jerrams, Investigation into the electromechanical properties of dielectric elastomers subjected to pre-stressing, Mater. Sci. Eng. C 49 (2015) 754–760.
[35] P. Kim, S.C. Jones, P.J. Hotchkiss, J.N. Haddock, B. Kippelen, S.R. Marder, et al., Phosphonic acid-modified barium titanate polymer nanocomposites with high permittivity and dielectric strength, Adv. Mater. 19 (2007) 1001–1005.
[36] M. Molberg, D. Crespy, P. Rupper, F. Nüesch, J.-A.E. Månson, C. Löwe, et al., High breakdown field dielectric elastomer actuators using encapsulated polyaniline as high dielectric constant filler, Adv. Funct. Mater. 20 (2010) 3280–3291.
[37] J.E.Q. Quinsaat, M. Alexandru, F.A. Nuesch, H. Hofmann, A. Borgschulte, D.M. Opris, Highly stretchable dielectric elastomer composites containing high volume fractions of silver nanoparticles, J. Mater. Chem. A 3 (2015) 14675–14685.
[38] D. Yang, Y. Ni, X. Kong, Y. Wang, L. Zhang, A mussel-like inspired modification of BaTiO3 nanopartciles using catechol/polyamine co-deposition and silane grafting for high-performance dielectric elastomer composites, Compos. Part B 172 (2019) 621–627.
[39] Y. Liu, K. Ai, L. Lu, Polydopamine and its derivative materials: synthesis and promising applications in energy, environmental, and biomedical fields, Chem. Rev. 114 (2014) 5057–5115.
[40] D. Yang, M. Ruan, S. Huang, Y. Wu, S. Li, H. Wang, et al., Dopamine and silane functionalized barium titanate with improved electromechanical properties for silicone dielectric elastomers, RSC Adv. 6 (2016) 90172–90183.
[41] A.E. Matthew, S. Andrew, H. Pine, L.U. Sandra, M.D. Abhaya, Characterization of polyphenol oxidase from walnut, J. Am. Soc. Hortic. Sci. 133 (2008) 852–858.
[42] C. Sánchez-González, C.J. Ciudad, V. Noé, M. Izquierdo-Pulido, Health benefits of walnut polyphenols: an exploration beyond their lipid profile, Crit. Rev. Food Sci. Nutr. 57 (2017) 3373–3383.
[43] J. Regueiro, C. Sánchez-González, A. Vallverdú-Queralt, J. Simal-Gándara, R. Lamuela-Raventós, M. Izquierdo-Pulido, Comprehensive identification of walnut polyphenols by liquid chromatography coupled to linear ion trap–Orbitrap mass spectrometry, Food Chem. 152 (2014) 340–348.
[44] S.A. Haddadi, T.B. Kohlan, S. Momeni, A. Ramazani S.A, M. Mahdavian, Synthesis and application of mesoporous carbon nanospheres containing walnut extract for fabrication of active protective epoxy coatings, Progress in Organic Coatings, 133(2019) 206–19.
[45] G. Mathew, J.M. Rhee, C. Nah, D.J. Leo, Effects of silicone rubber on properties of dielectric acrylate elastomer actuator, Polym. Eng. Sci. 46 (2006) 1455–1460.
[46] B. Luo, X. Wang, Y. Wang, L. Li, Fabrication, characterization, properties and theoretical analysis of ceramic/PVDF composite flexible films with high dielectric constant and low dielectric loss, J. Mater. Chem. A 2 (2014) 510–519.
[47] S. Tangwiwat, S.J. Milne, Barium titanate sols prepared by a diol-based sol–gel route, J. Non-Cryst. Solids 351 (2005) 976–980.
[48] R. Ashiri, Detailed FT-IR spectroscopy characterization and thermal analysis of synthesis of barium titanate nanoscale particles through a newly developed process, Vib. Spectrosc. 66 (2013) 24–29.
[49] M. Nasrollahzadeh, M. Atarod, B. Jaleh, M. Gandomirouzbahani, In situ green synthesis of Ag nanoparticles on graphene oxide/TiO2 nanocomposite and their catalytic activity for the reduction of 4-nitrophenol, congo red and methylene blue, Ceram. Int. 42 (2016) 8587–8596.
[50] J. Mihály, R. Deák, I.C. Szigyártó, A. Bóta, T. Beke-Somfai, Z. Varga, Characterization of extracellular vesicles by IR spectroscopy: fast and simple classification based on amide and CH stretching vibrations, Biochim. Biophys. Acta Biomembr. 1859 (2017) 459–466.
[51] W. Du, J. Liu, Z. Li, High self-dispersibility carbon black particles prepared via hydroxylation and urethane chains encapsulation for enhancing properties of waterborne polyurethane composite films, Colloids Surf. A Physicochem. Eng. Asp. 543 (2018) 46–55.
[52] D. Yang, M. Tian, D. Li, W. Wang, F. Ge, L. Zhang, Enhanced dielectric properties and actuated strain of elastomer composites with dopamine-induced surface functionalization, J. Mater. Chem. A 1 (2013) 12276–12284.
[53] W. Lei, R. Wang, D. Yang, G. Hou, X. Zhou, H. Qiao, et al., Design and preparation of bio-based dielectric elastomer with polar and plasticized side chains, RSC Adv. 5 (2015) 47429–47438.
[54] J. Fu, Y. Hou, M. Zheng, Q. Wei, M. Zhu, H. Yan, Improving dielectric properties of PVDF composites by employing surface modified strong polarized BaTiO3 particles derived by molten salt method, ACS Appl. Mater. Interfaces 7 (2015) 24480–24491.
[55] F. Wen, Z. Xu, S. Tan, W. Xia, X. Wei, Z. Zhang, Chemical bonding-induced low dielectric loss and low conductivity in high-K poly(vinylidenefluoride-trifluorethylene)/graphene nanosheets nanocomposites, ACS Appl. Mater. Interfaces 5 (2013) 9411–9420.
[56] L. Xie, X. Huang, C. Wu, P. Jiang, Core-shell structured poly(methyl methacrylate)/BaTiO3 nanocomposites prepared by in situ atom transfer radical polymerization: a route to high dielectric constant materials with the inherent low loss of the base polymer, J. Mater. Chem. 21 (2011) 5897–5906.
[57] C.O. Horgan, G. Saccomandi, A description of arterial wall mechanics using limiting chain extensibility constitutive models, Biomechan Model Mechanobiol 1 (2003) 251–266.
[58] S.J.A. Koh, C. Keplinger, R. Kaltseis, C.-C. Foo, R. Baumgartner, S. Bauer, et al., High-performance electromechanical transduction using laterally-constrained dielectric elastomers part I: actuation processes, Journal of the Mechanics and Physics of Solids 105 (2017) 81–94.
[59] O. Yeoh, P. Fleming, A new attempt to reconcile the statistical and phenomenological theories of rubber elasticity, Journal of Polymer Science-B-Polymer Physics Edition 35 (1997) 1919–1932.
[60] X.H. Zhao, Z.G. Suo, Theory of dielectric elastomers capable of giant deformation of actuation, Phys. Rev. Lett. 104 (2010) 4.
[61] T. Lu, J. Huang, C. Jordi, G. Kovacs, R. Huang, D.R. Clarke, et al., Dielectric elastomer actuators under equal-biaxial forces, uniaxial forces, and uniaxial constraint of stiff fibers, Soft Matter 8 (2012) 6167–6173.
[62] Q. Guo, Y. Chen, J. Zhang, Z. Yao, Large impact in electrical properties of polypropylene by improving the filler-matrix interface effect in PP/PS blends, Polym. Test. 63 (2017) 587–595.